

Synthesis and Characterization of Porous Benzimidazole-Linked Polymers and Their Performance in Small Gas Storage and Selective Uptake

Mohammad Gulam Rabbani and Hani M. El-Kaderi*

Department of Chemistry, Virginia Commonwealth University, Richmond, VA, 23284-2006, USA

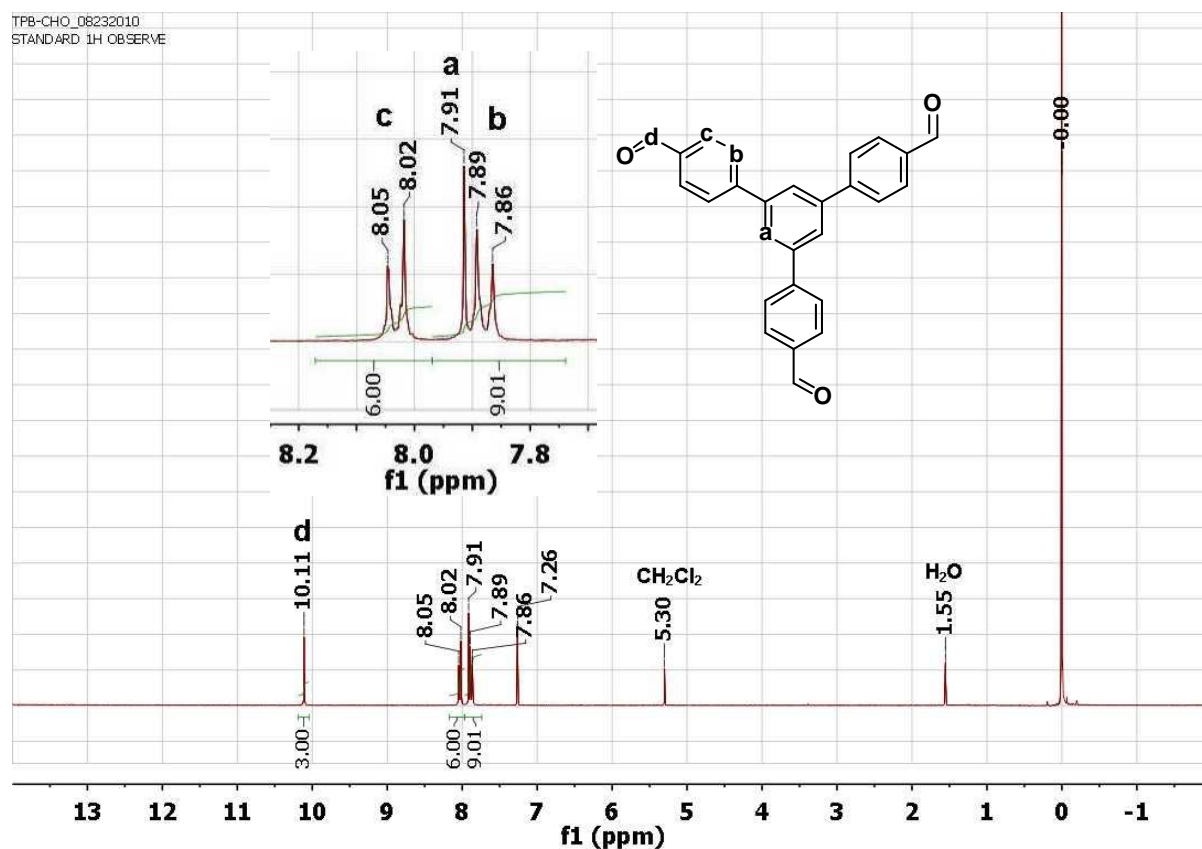
*To whom correspondence should be addressed. E-Mail: helkaderi@vcu.edu

Table of Contents

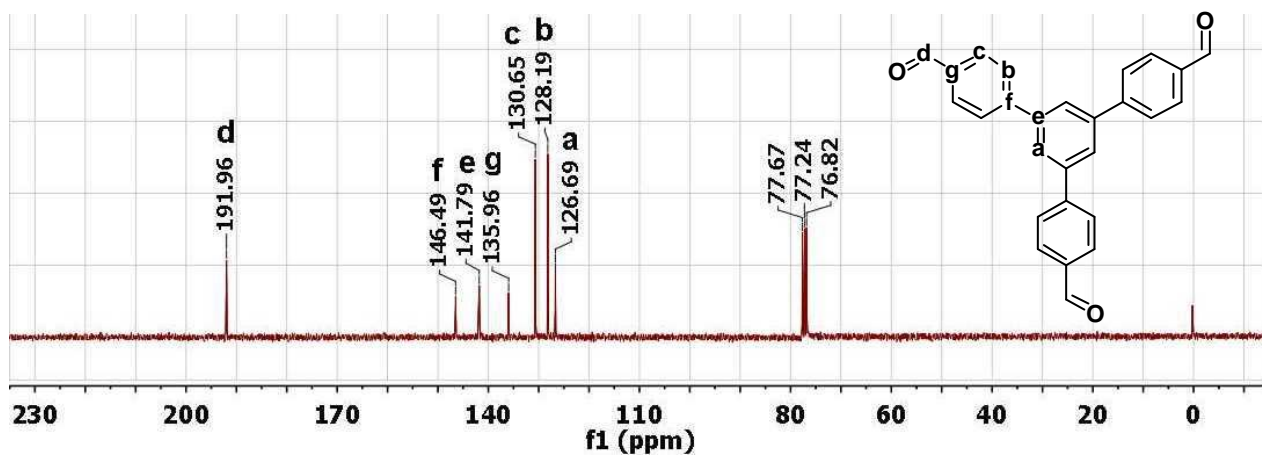
Section S1:	<i>NMR spectral Characterization of Starting Building Units</i>	2
Section S2:	<i>Synthesis and Characterization of BILPs</i>	6
	<i>Thermogravimetric Analysis</i>	7
	<i>Scanning Electron Microscopy Imaging (SEM)</i>	8
	<i>XRD-pattern for BILPs.</i>	9
	<i>FT-IR Spectroscopy of Starting Materials and BILPs</i>	10
	<i>Solid state ^{13}C CP-MAS NMR spectrum for BILPs</i>	11
Section S3:	<i>Low-Pressure (0 – 1.0 bar) Gas Adsorption Measurements for BILPs</i>	13

Section S1: NMR spectral Characterization of Starting Building Units

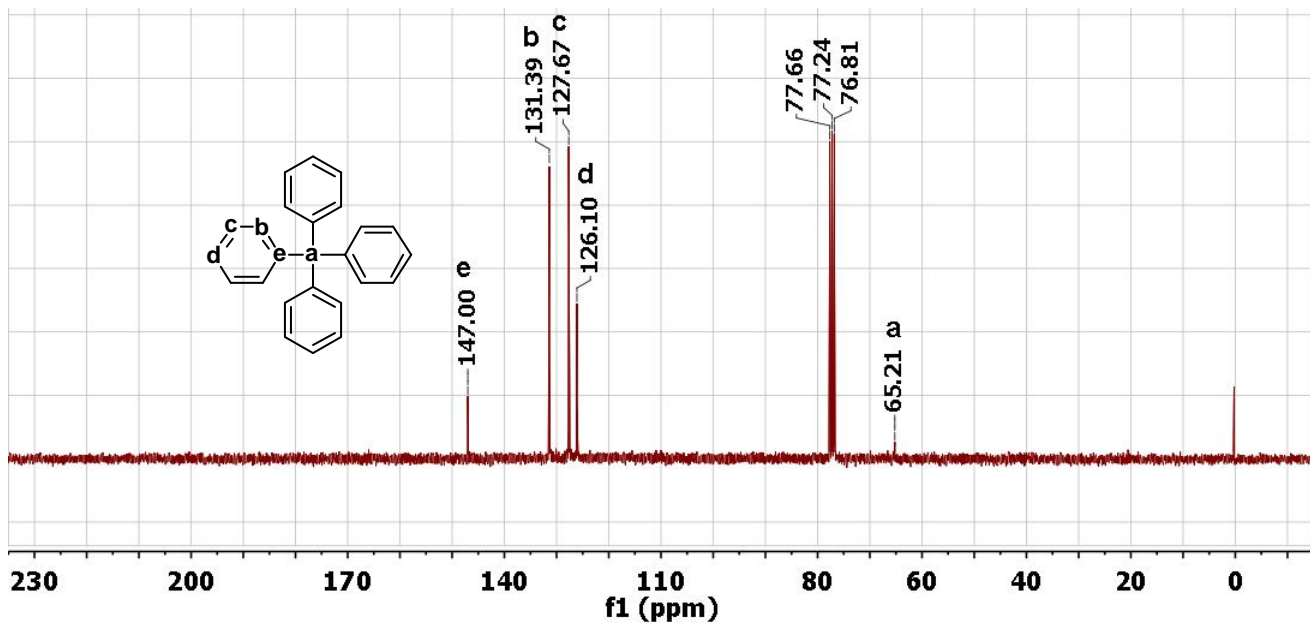
¹H NMR for 1,3,5-tris(4-formylphenyl)benzene (TFPB) in CDCl₃:



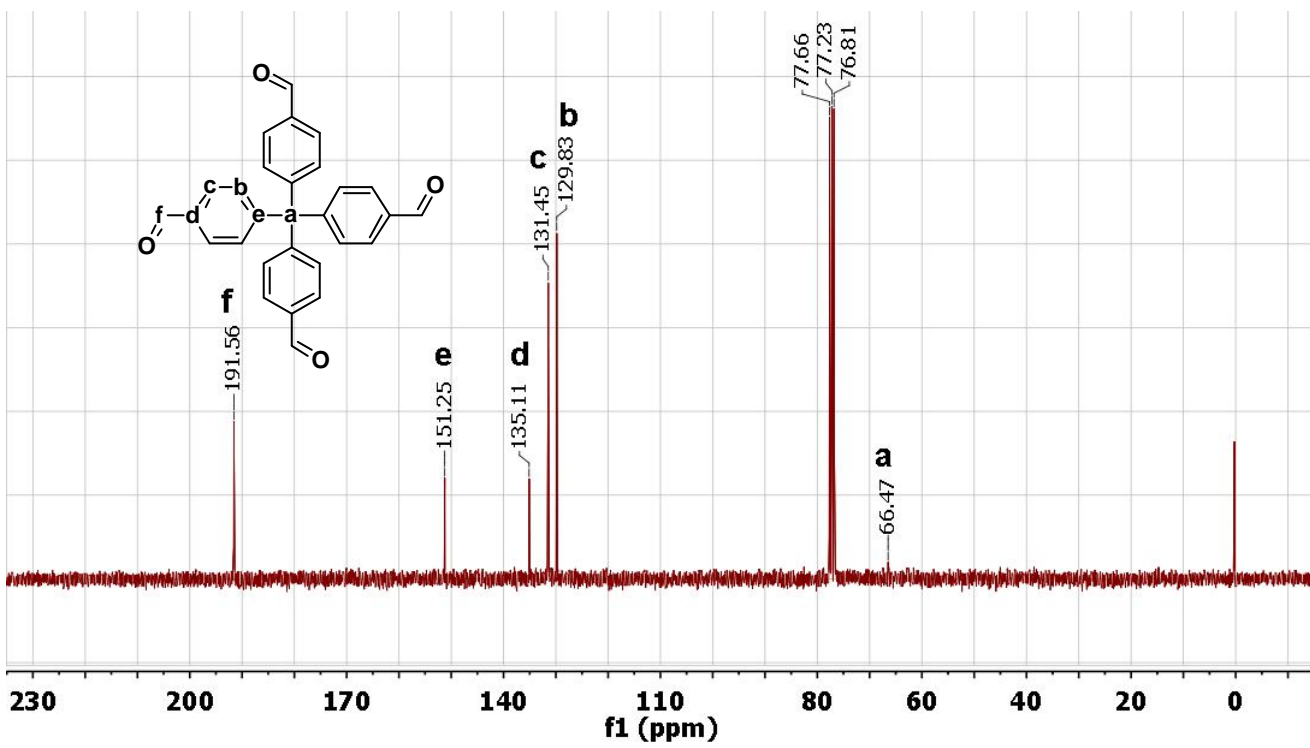
¹³C NMR for 1,3,5-tris(4-formylphenyl)benzene (TFPB) in CDCl₃:



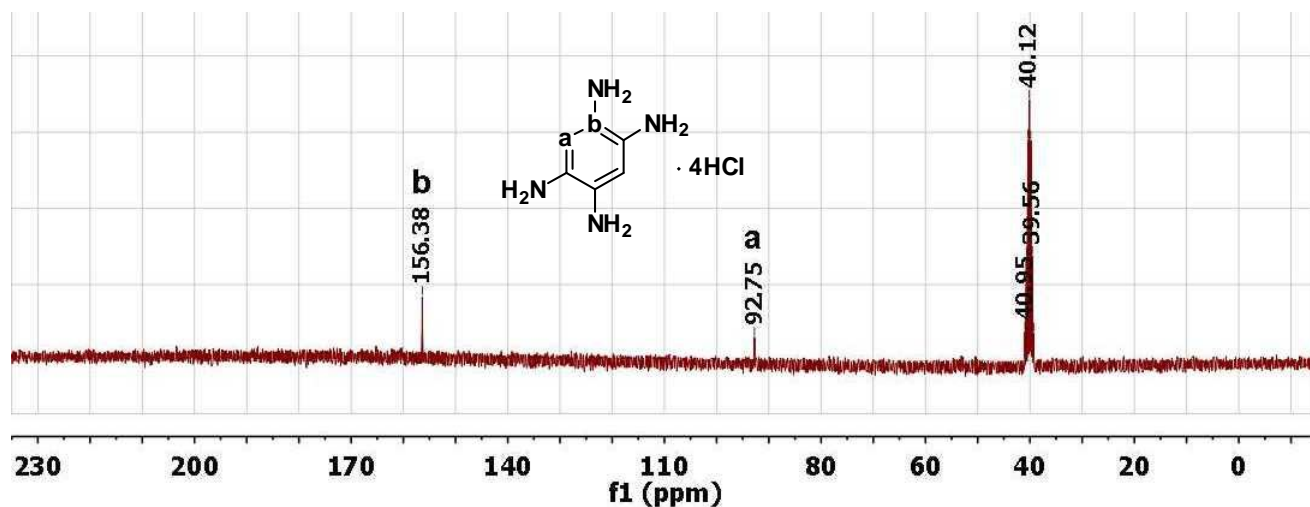
^{13}C NMR for Tetraphenylmethane (TPM) in CDCl_3 :



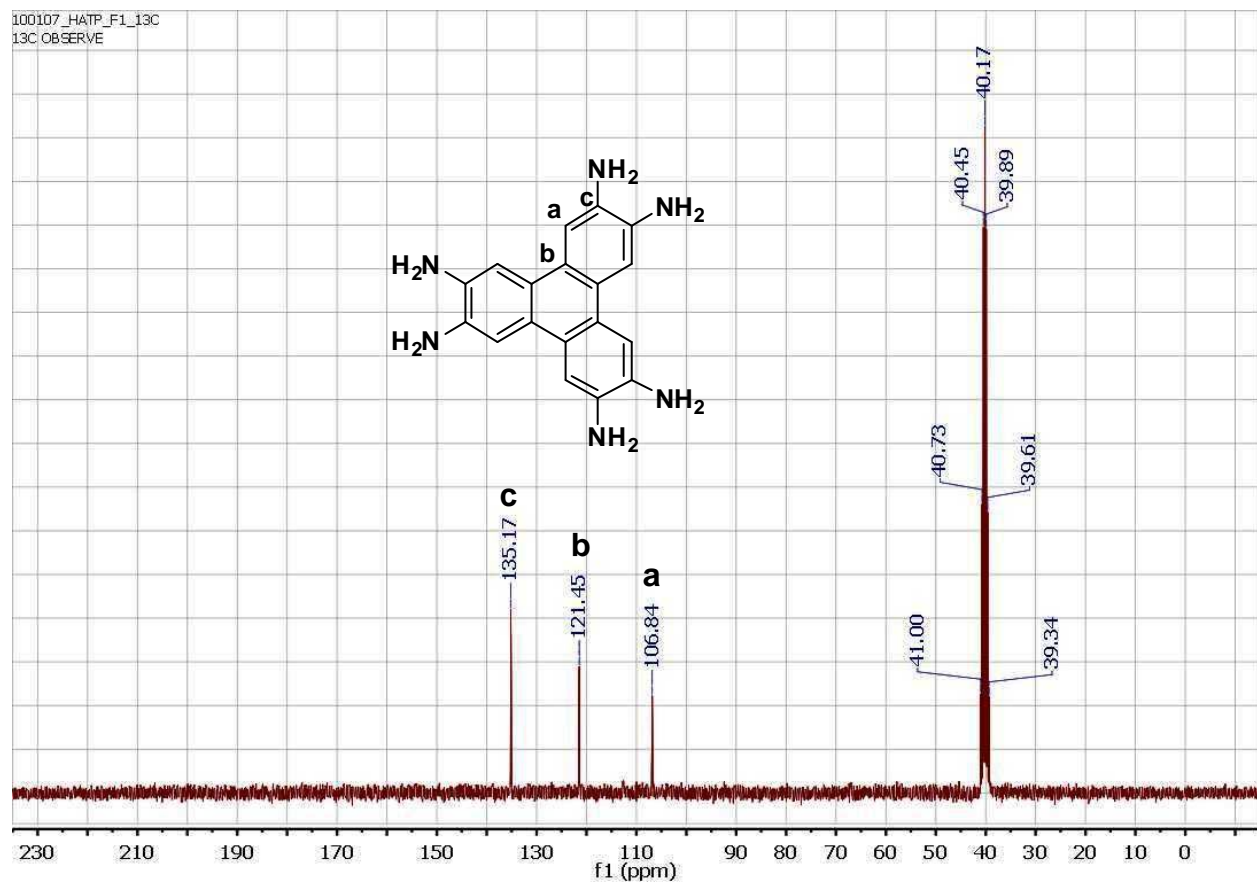
^{13}C NMR for Tetrakis(4-formylphenyl)methane (TFPM) in CDCl_3 :



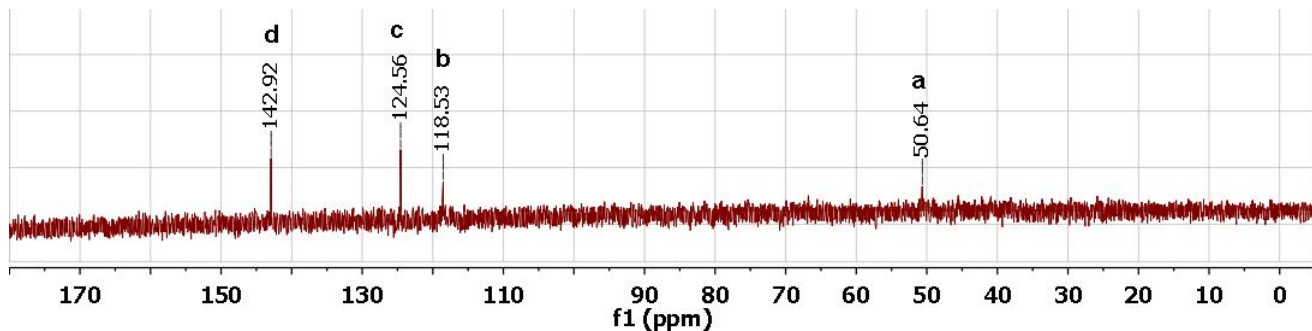
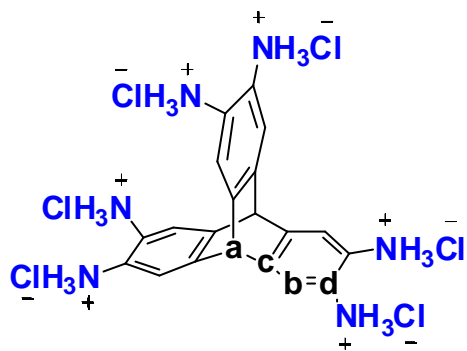
¹³C NMR for benzenetetramine (BTA) tetrahydrochloride (in *d*₆ DMSO)



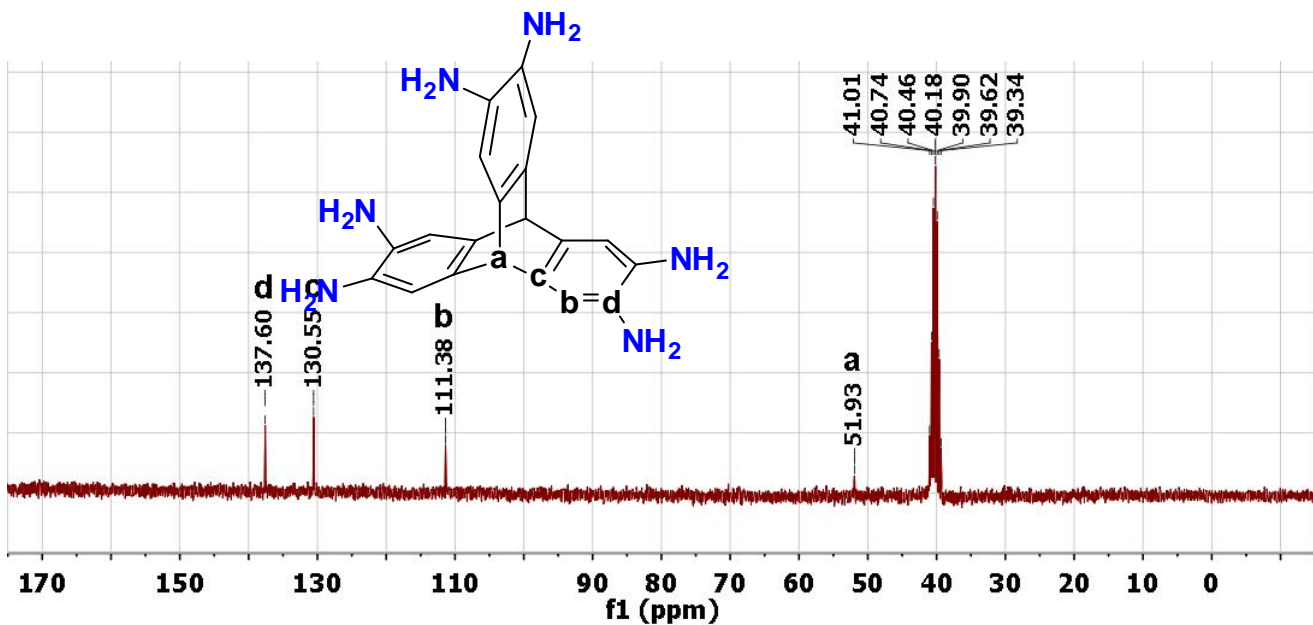
¹³C NMR spectrum of HATP (in *d*₆ DMSO).



^{13}C NMR for 2,3,6,7,14,15-Hexaaminotriptycene hexahydrochloride in D_2O .



^{13}C NMR for 2,3,6,7,14,15-Hexaaminotriptycene (HATT) $\text{DMSO}-d_6$:



Section 2: Synthesis and Characterization of BILPs

Scheme S1: Synthesis of BILPs

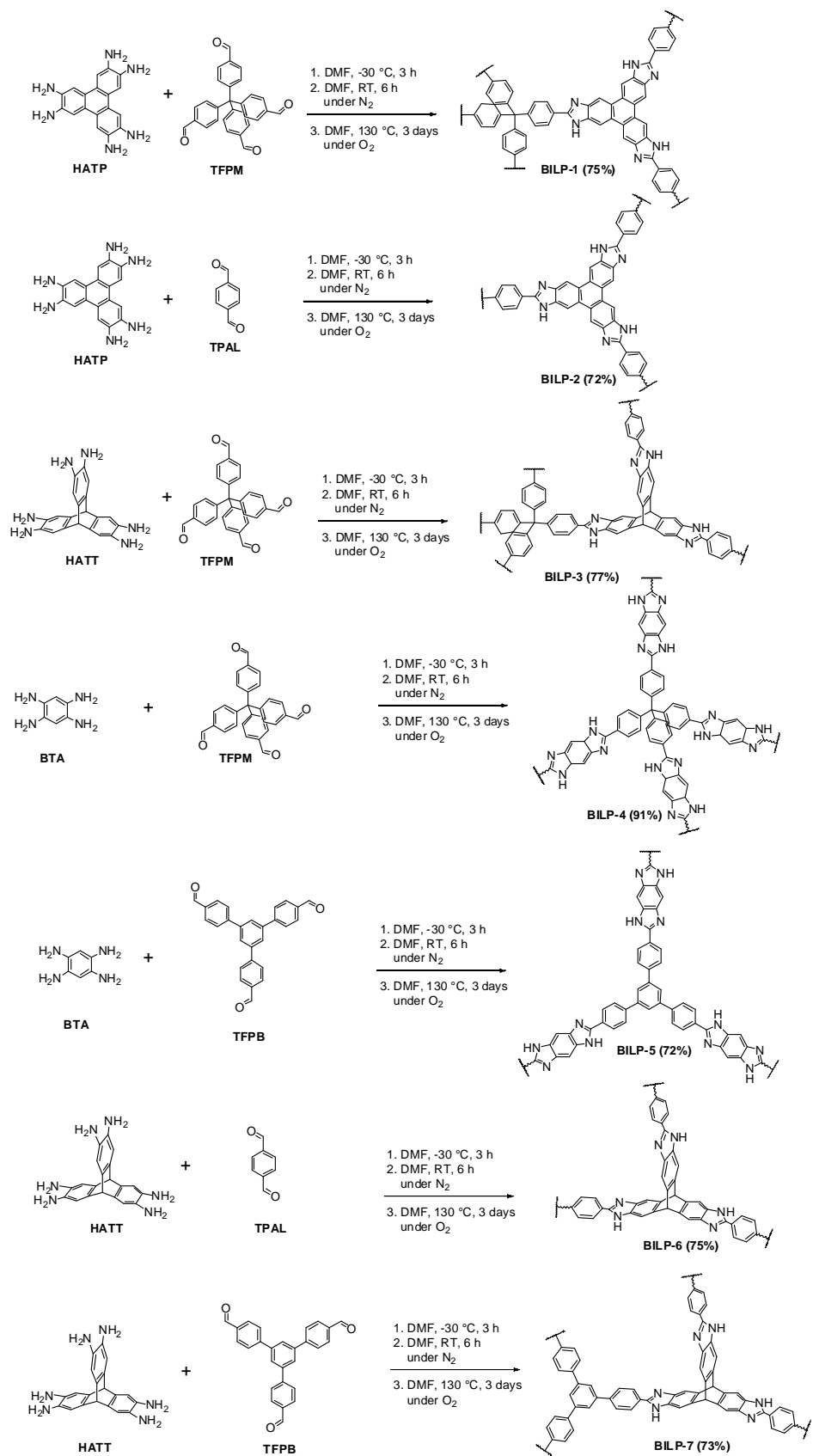


Figure S1: TGA traces of BILP-2, BILP-4, BILP-5 and BILP-7.

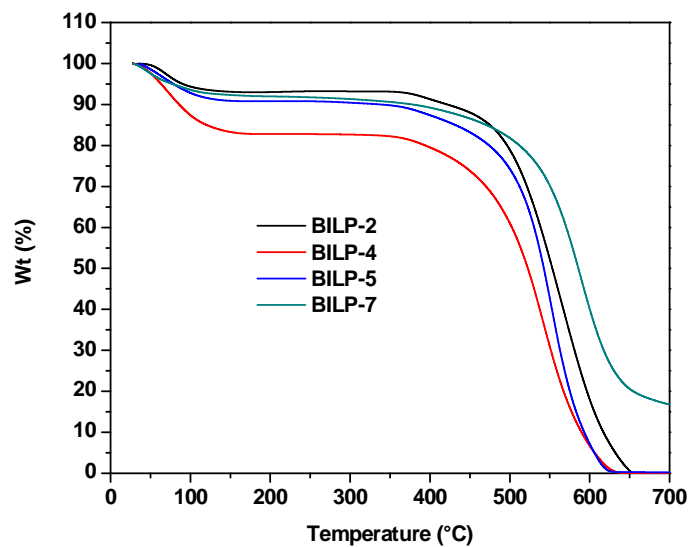
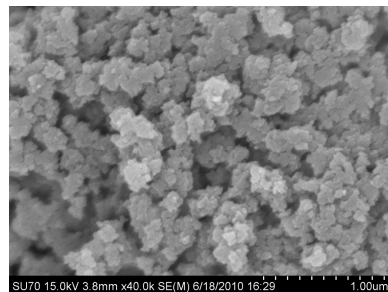
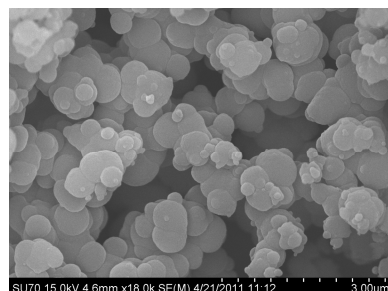


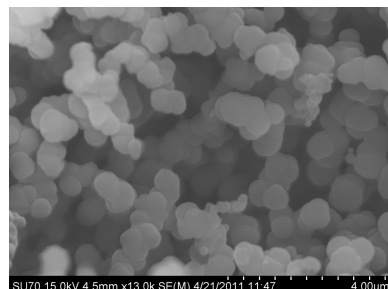
Figure S2: SEM image of BILP-2, BILP-4, BILP-5 and BILP-7.



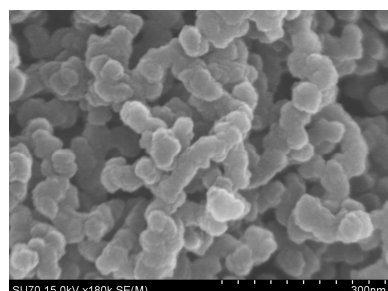
BILP-2: Aggregated particles 400-600 nm size



BILP-4: Aggregated spherical particles 3-5 micrometer



BILP-5: Aggregated spherical particles 4-6 micrometer



BILP-7: Spherical particles (300-350 nm) aggregate to form coral reef type morphology

Figure S3: XRD-pattern for BILPs. Intense peak at 28 is due to the surface characteristics of sample holder. The broad peak at around $2\theta = 15$ indicates the amorphous characteristics of BILPs.

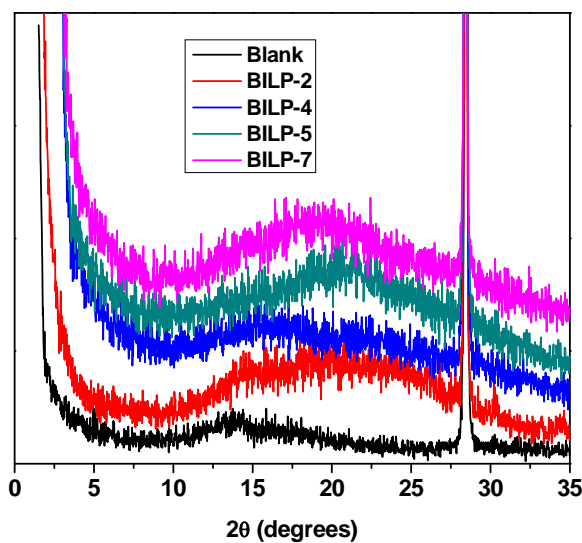


Figure S4: FT-IR spectra of BILPs and their starting building units. Lower panel is an expanded region from 400 to 2000 cm⁻¹. Spectra of BILPs showed N-H stretching at around 3415 cm⁻¹ (free N-H) and 3215 cm⁻¹ (hydrogen bonded N-H), while new bands appeared at 1612 cm⁻¹ (C=N), and 1495 and 1435 cm⁻¹ which can be assigned to skeleton vibration of the benzimidazole ring. The new band at around 1355 cm⁻¹ can be assigned to C-N stretching for benzimidazole ring, while 1637 cm⁻¹ band is due to the NH bendings. The bands ranging 2870-3050 cm⁻¹ are due to aromatic CH stretching. Trace of C=O stretching band at around 1700 cm⁻¹ in BILPs indicates the residual terminal aldehyde functional group in polymers.

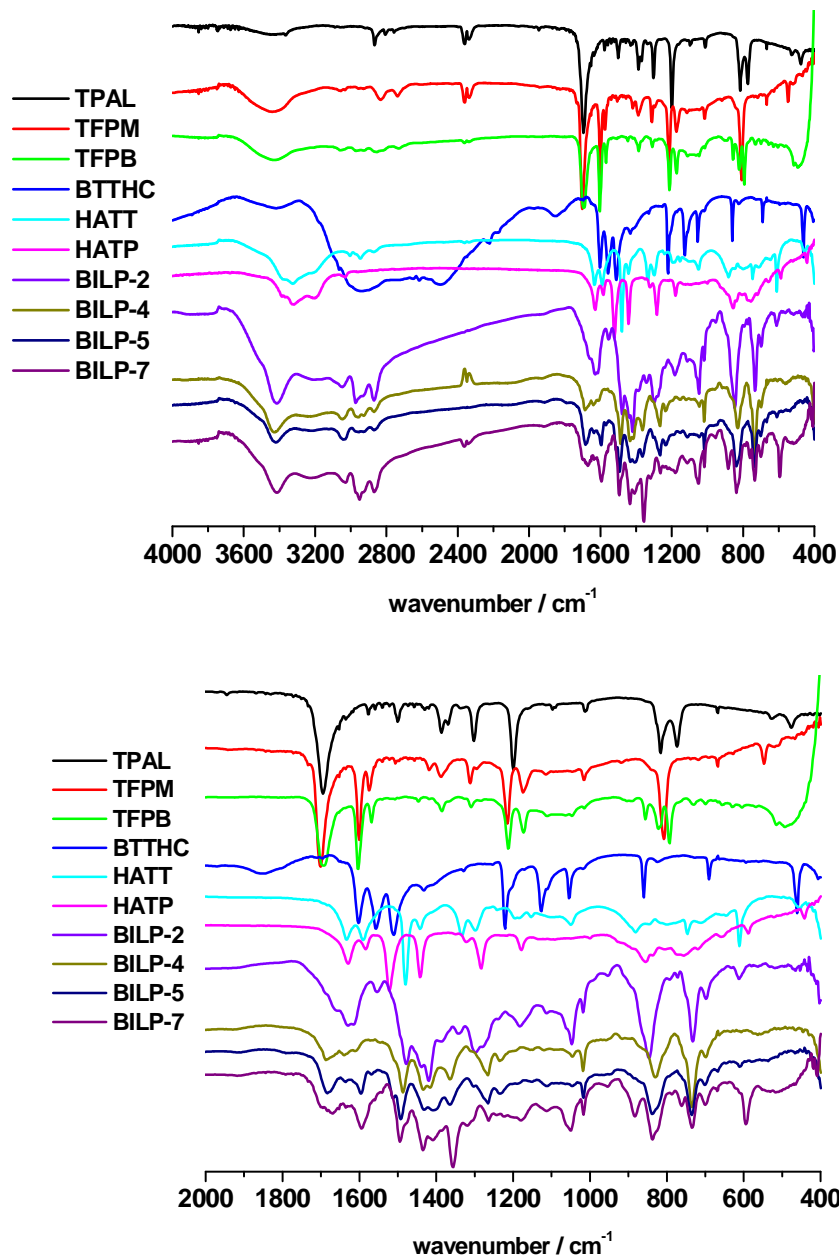


Figure S5: Solid state ^{13}C CP-MAS NMR spectra of BILP-2, BILP-4, BILP-5 and BILP-7.

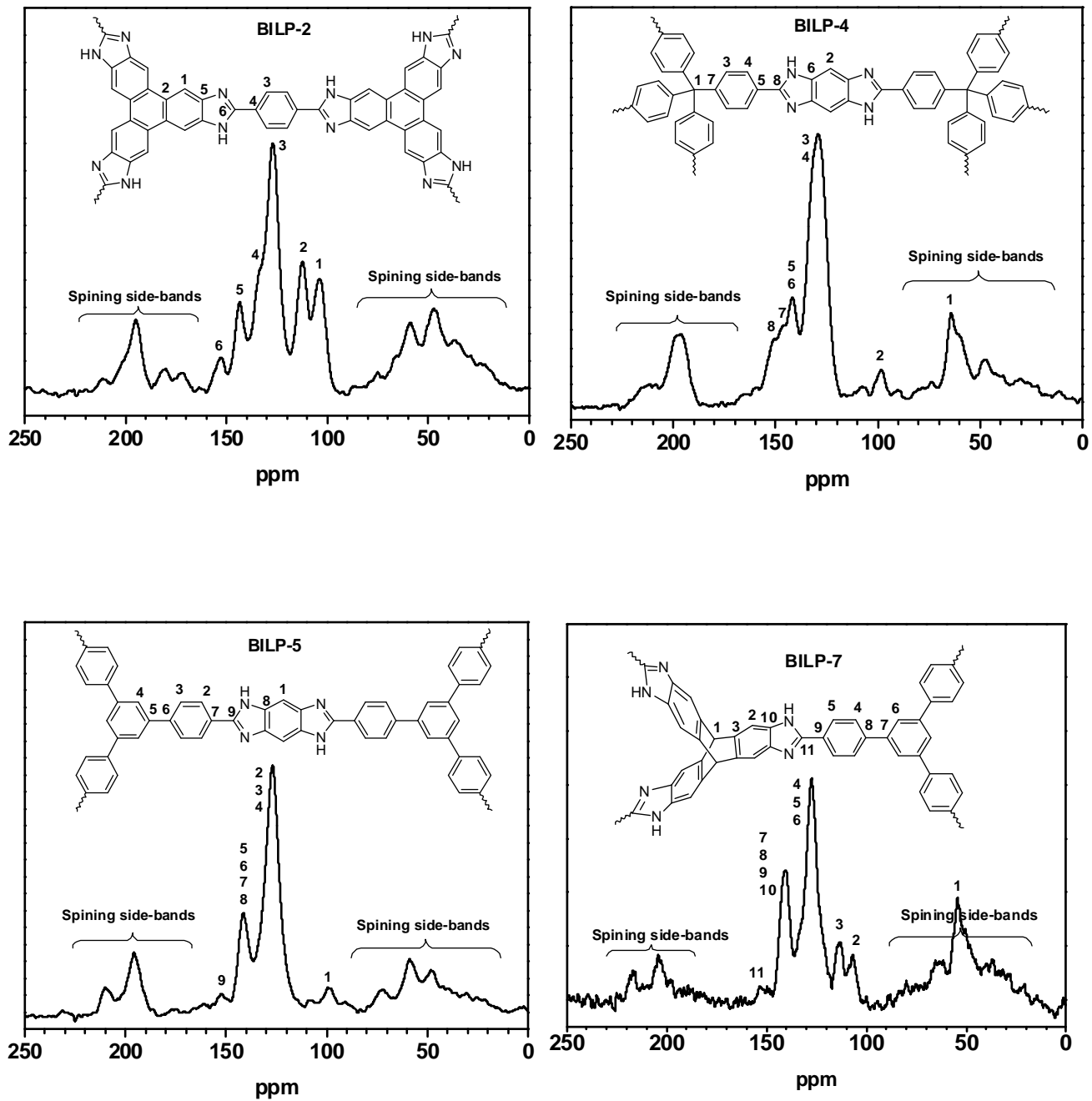


Table S1. Assignments of the ^{13}C CP-MAS NMR peaks for BILPs.

Peaks (ppm)							Assignments/comments
BILP-1	BILP-2	BILP-3	BILP-4	BILP-5	BILP-6	BILP-7	
		55			54	54	Triptycene aliphatic CH (1)
65		64	64				Quaternary C for tetraphenyl methane building block. This quaternary carbon usually gives weak peak and this is overlapped here by spinning side-bands.
			99	99			This CH is observed at 93 ppm in benzenetetramine tetrahydrochloride.
104	104						Triphenylene aromatic CH (1). This is observed at 107 ppm in HATP (d_6 -DMSO).
		105			106	107	Triptycene aromatic CH (2). This is observed at 111 ppm in HATT (d_6 -DMSO).
112	112						Triphenylene aromatic C (2). This is observed at 121 ppm in HATP (d_6 -DMSO).
		114			113	113	Triptycene aromatic C (3). This is observed at 131 ppm in HATT (d_6 -DMSO).
127 (br)	127 (br)	130 (br)	129 (br)	127 (br)	128 (br)	127 (br)	Aromatic CH.
135(sh), 144	134(sh), 144	140 (sh), 142	142, 146	140(sh), 141	139 (sh), 141	141	Aromatic C.
152	153	152	151	152	151	152	Benzimidazole ring C in C=N. It is noted that no peak was observed at around 160 ppm for imine C=N. This suggests the successful formation of benzimidazole ring. ^{7,9}

Section 3: Low-Pressure (0 – 1.0 bar) Gas Adsorption Measurements for BILPs.

Activation of BILPs for gas adsorption measurements: A sample was loaded into a 9 mm large bulb cell (from Quantachrome) of known weight and then hooked up to MasterPrep. The sample was degassed at 120 °C for 12 hours. The degassed sample was weighed precisely and then transferred back to the analyzer. The temperatures for adsorption measurements was controlled by using refrigerated bath of liquid nitrogen (77 K) or liquid argon (87 K), and temperature controlled water bath (273 K and 298K). Adsorption measurements were performed on an Autosorb-1 C (Quantachrome) volumetric analyzer using adsorbates of UHP grade.

Figure S6: Ar adsorption isotherm for BILP-2 (black squares), BILP-4 (blue circles), BILP-5 (pink triangle) and BILP-7 (red diamond) measured at 87 K. The filled markers are adsorption points and the empty markers are desorption points.

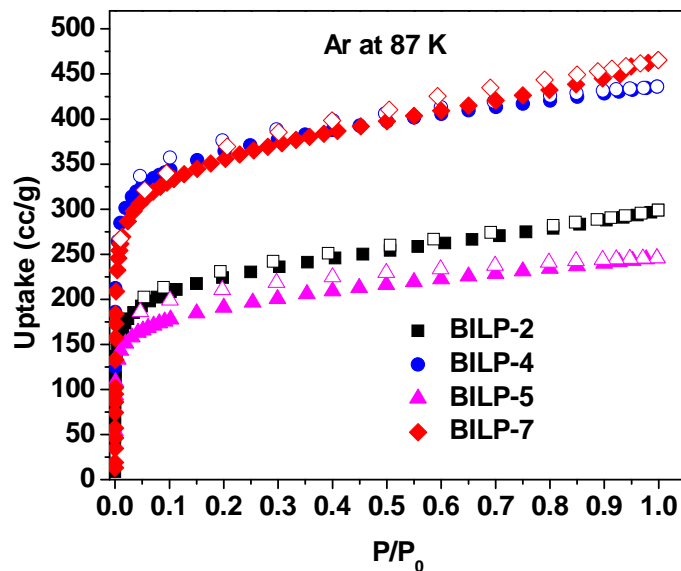


Figure S7: Experimental Ar adsorption isotherm (filled circles) for BILP-2, BILP-4, BILP-5 and BILP-7 measured at 87 K. The calculated NLDFT isotherm is overlaid as open circle. Note that a fitting error of < 1 % indicates the validity of using this method for assessing the porosity of BILPs. The fitting error is indicated.

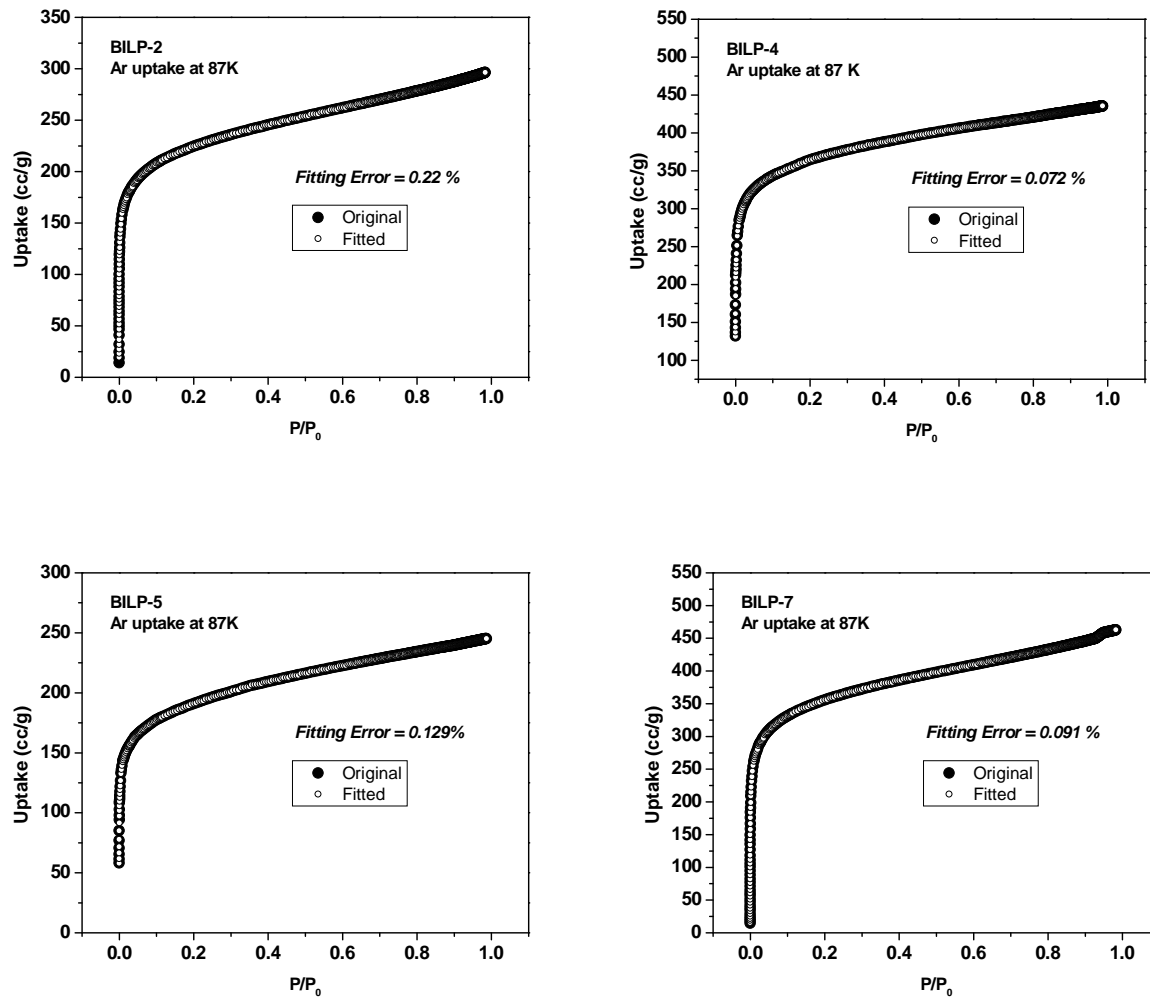


Figure S8: The Pore Size Distribution of BILPs was calculated from the Ar adsorption isotherms by the Non-Local Density Functional Theory (NLDFT) method using a cylindrical pore model.

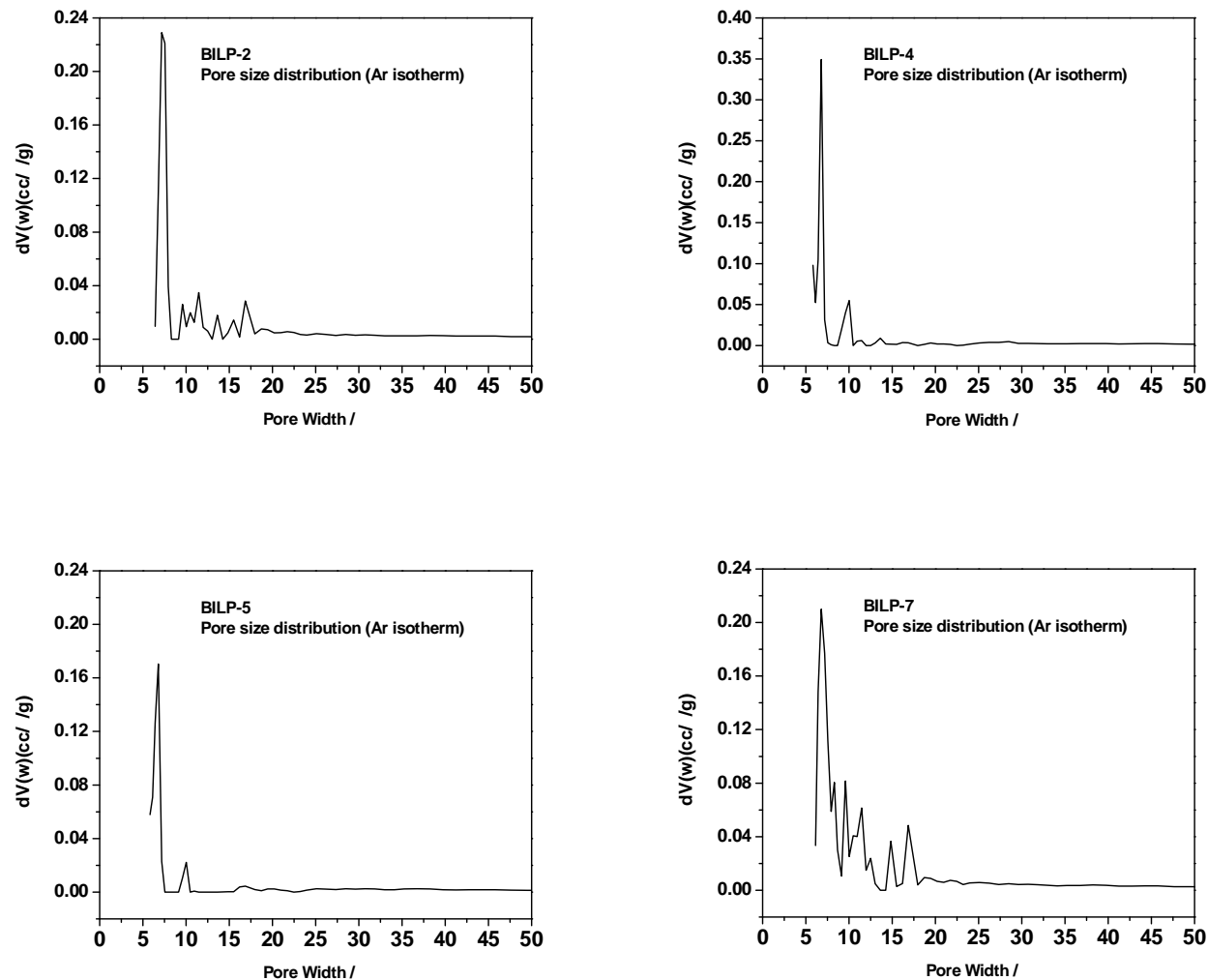


Figure S9: BET plots for BILP-2, BILP-4, BILP-5 and BILP-7 calculated from the Ar adsorption isotherm at 87 K. The model was applied from $P/P_0 = 0.05-0.15$. The correlation factor is indicated. ($W =$ Weight of gas absorbed at a relative pressure P/P_0).

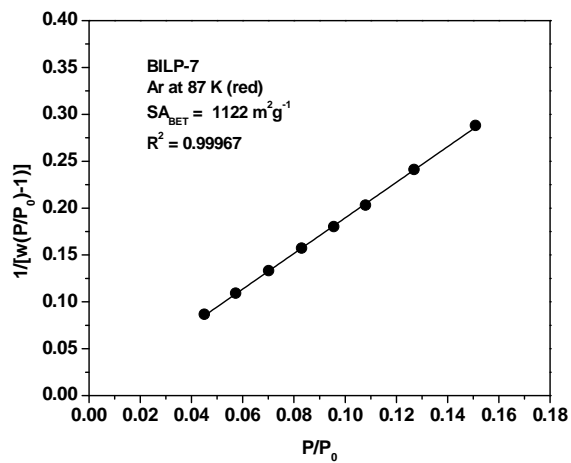
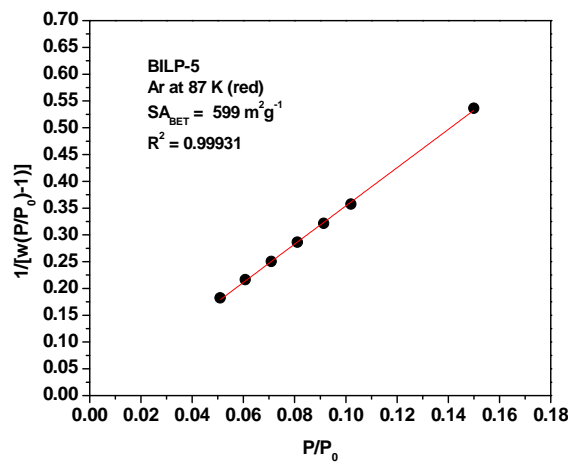
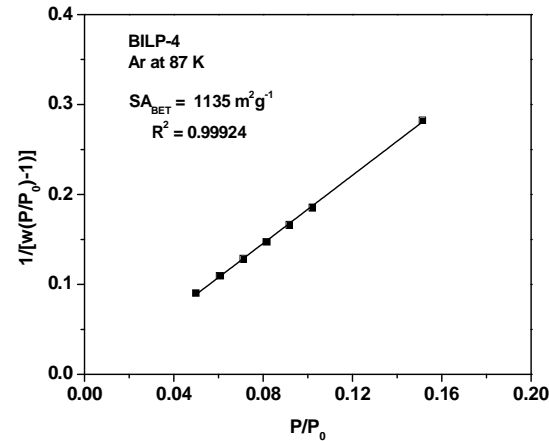
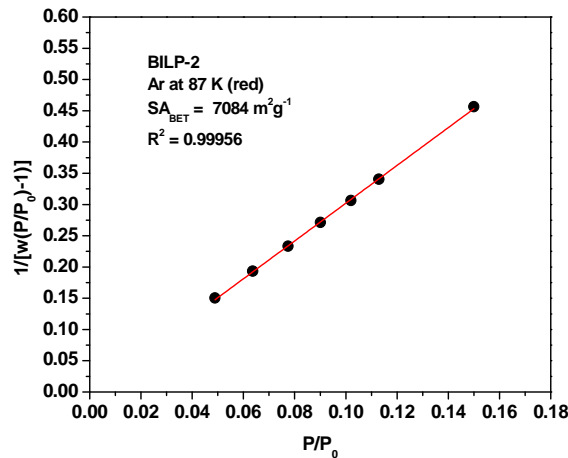


Figure S10: N₂ adsorption isotherm for BILP-2 (black squares), BILP-4 (blue circles), BILP-5 (pink triangle) and BILP-7 (red diamond) measured at 77 K. The filled markers are adsorption points and the empty markers are desorption points.

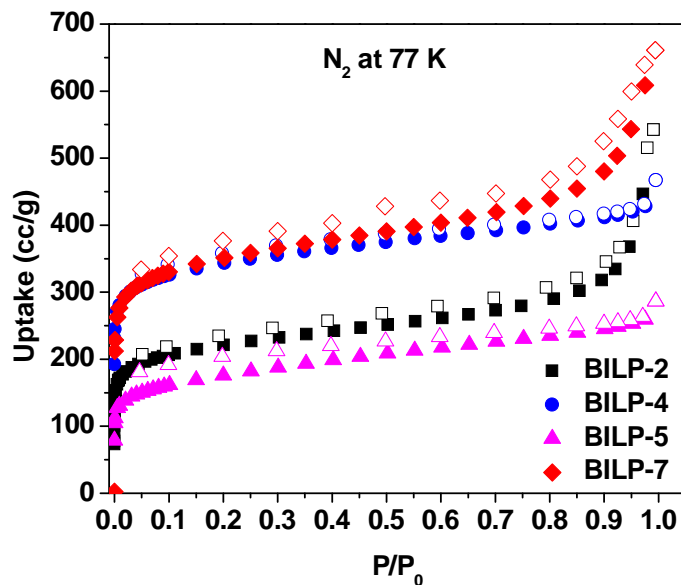


Figure S11: BET plots for BILP-2, BILP-4, BILP-5 and BILP-7 calculated from the N₂ adsorption isotherm at 77 K. The model was applied from P/P₀ = 0.05-0.15. The correlation factor is indicated. (W = Weight of gas absorbed at a relative pressure P/P₀).

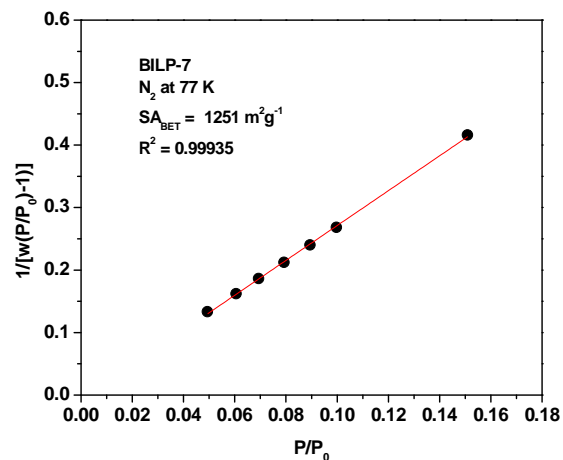
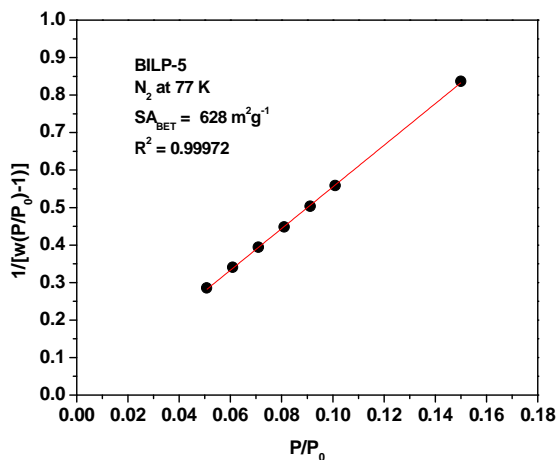
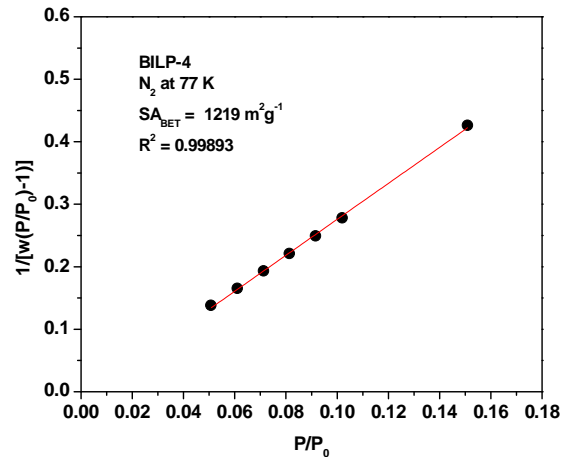
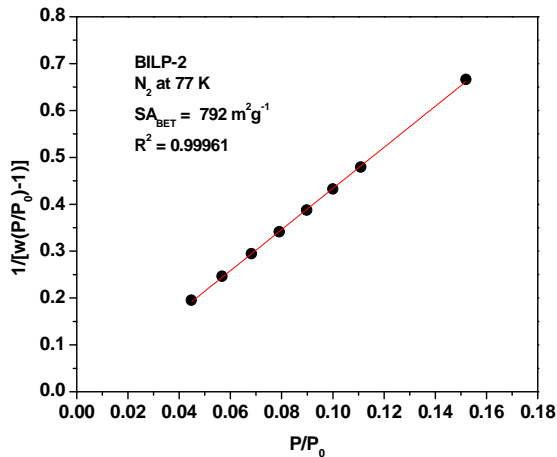


Figure S12: Gas uptake isotherms for BILP-2 (black squares), BILP-4 (blue circles), BILP-5 (pink triangle) and BILP-7 (red diamond) at 273 and 298 K.

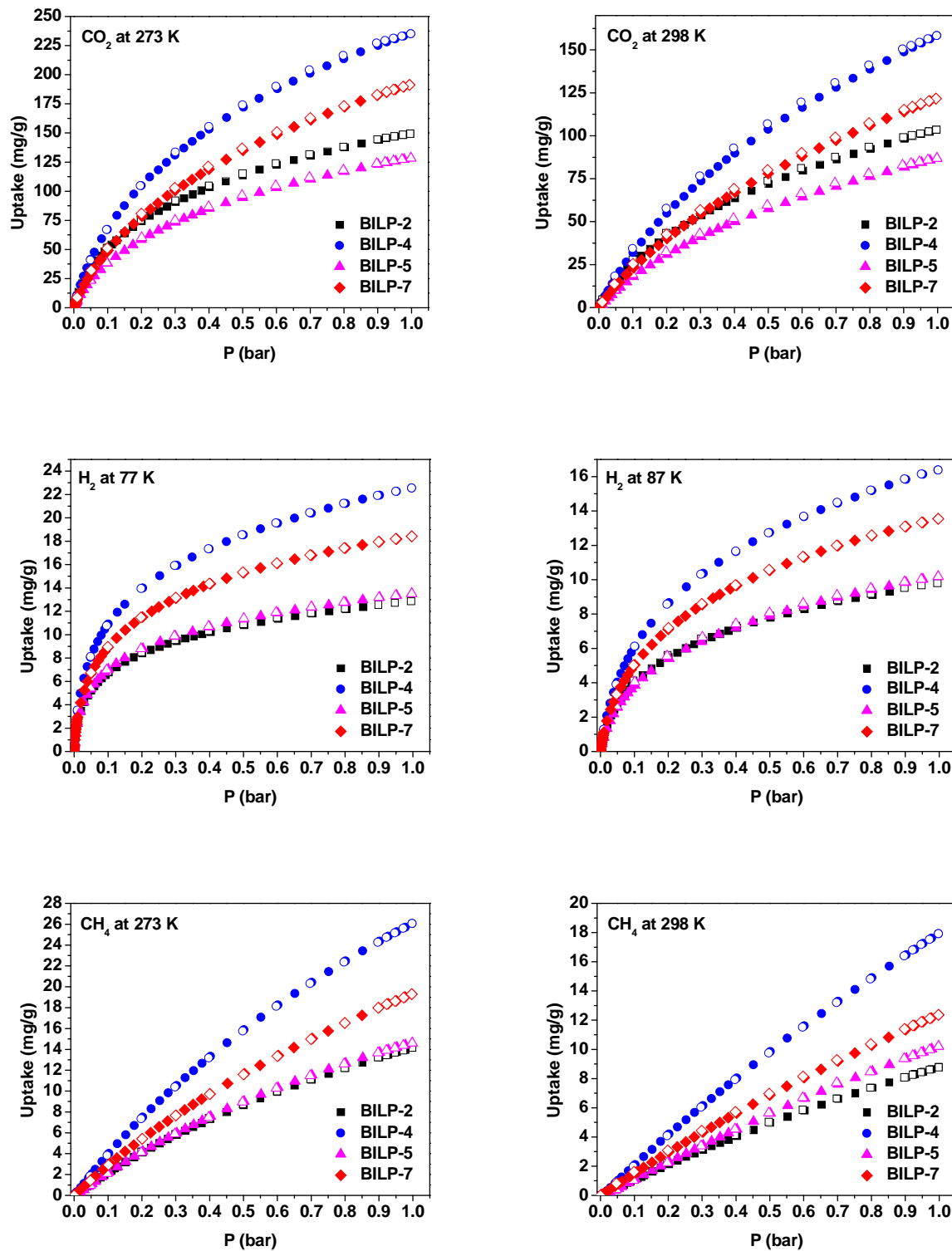


Figure S13: Virial analysis of CO₂ adsorption data for BILP-2, BILP-4, BILP-5 and BILP-7 (red circles: 273 K, blue squares: 298 K) and their isosteric heat of adsorption (Q_{st}).

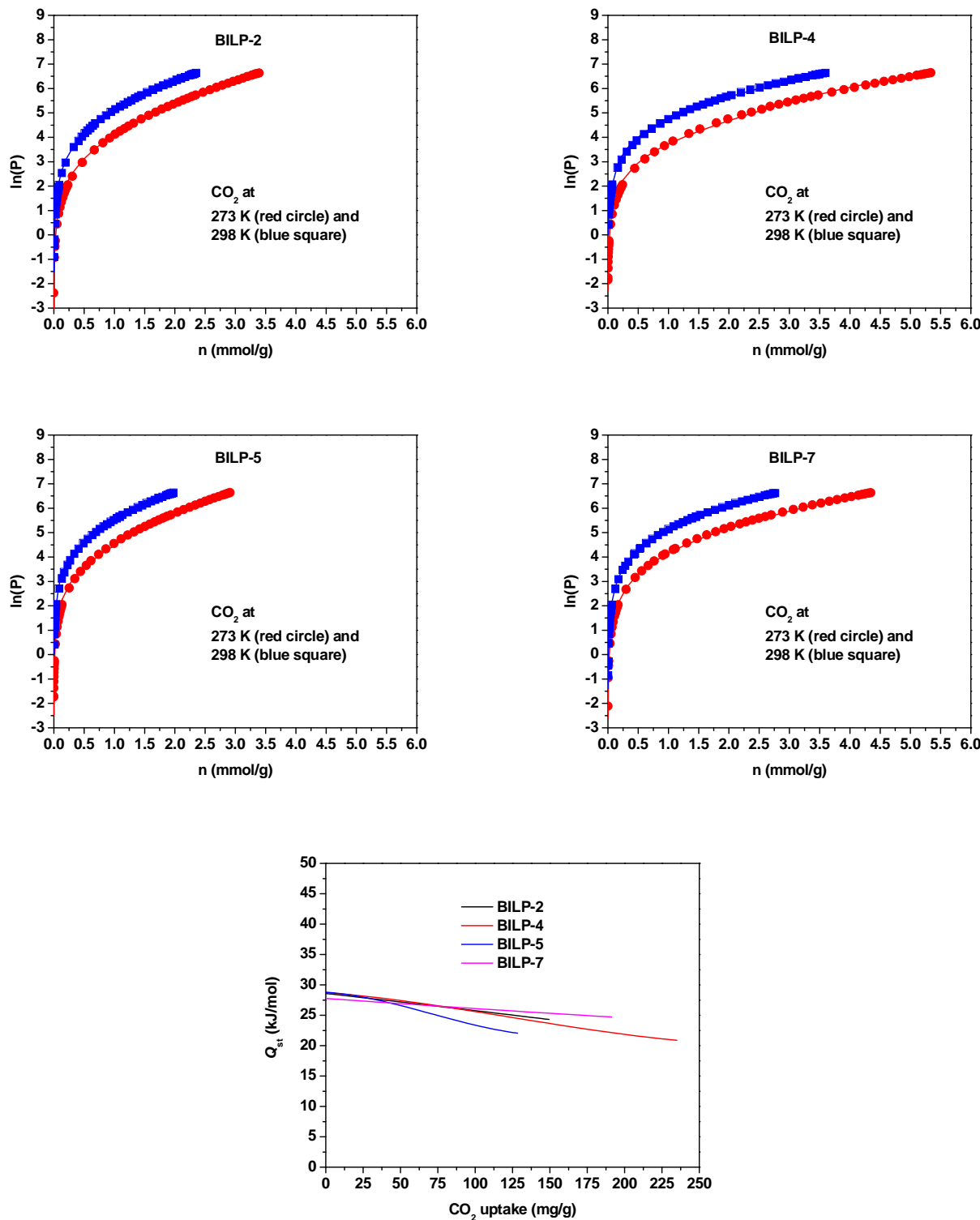


Figure S14: Virial analysis of H₂ adsorption data for BILP-2, BILP-4, BILP-5 and BILP-7 (red circles: 77 K, blue squares: 87 K) and their isosteric heat of adsorption (Q_{st}).

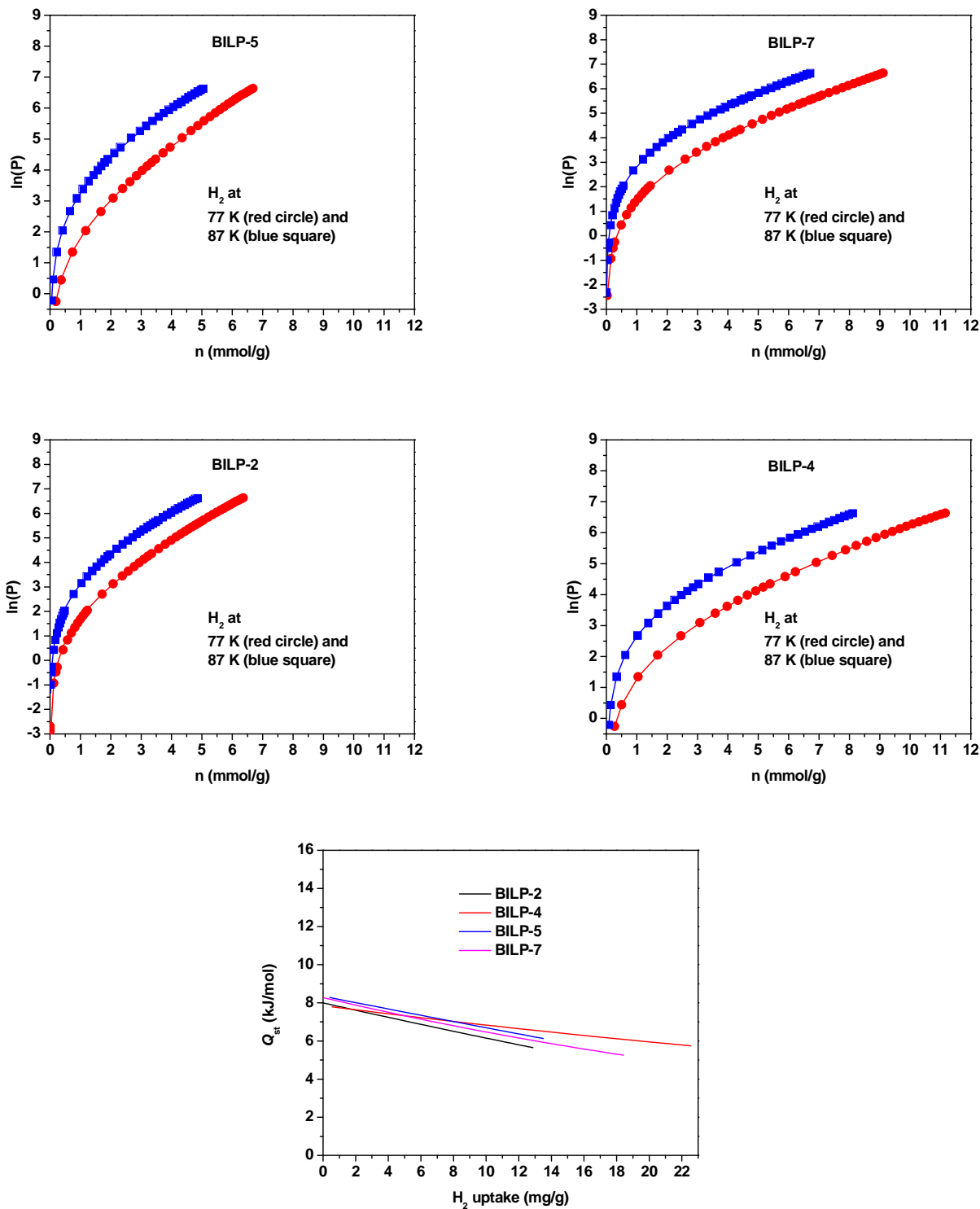


Figure S15: Virial analysis of CH_4 adsorption data for BILP-2, BILP-4, BILP-5 and BILP-7 (red circles: 273 K, blue squares: 298 K) and their isosteric heat of adsorption (Q_{st}).

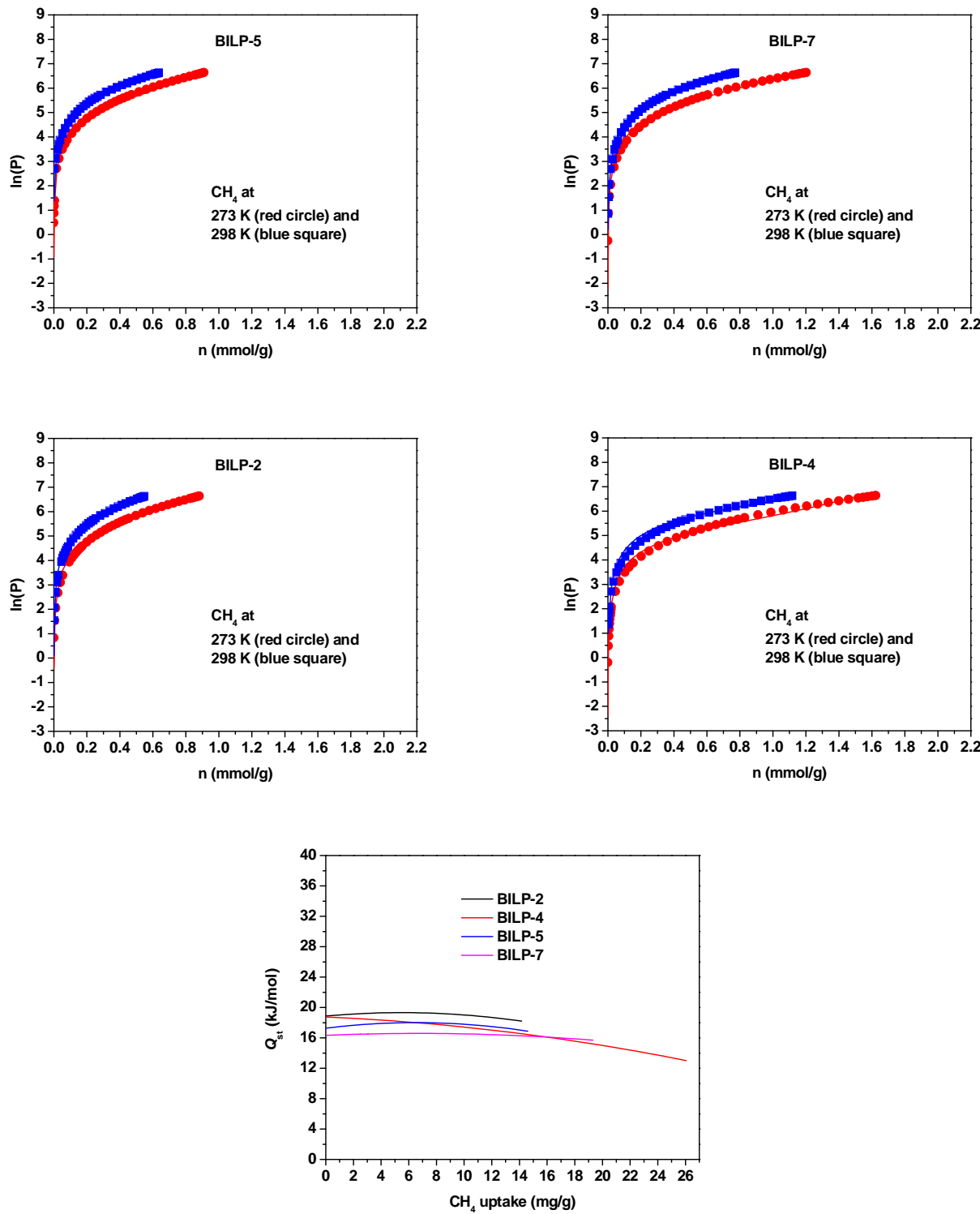


Figure S16: Gas sorption capacities for BILP-2, BILP-4, BILP-5 and BILP-7 at 273 and 298 K. CO_2 (black squares), CH_4 (red diamond) and N_2 (blue triangle).

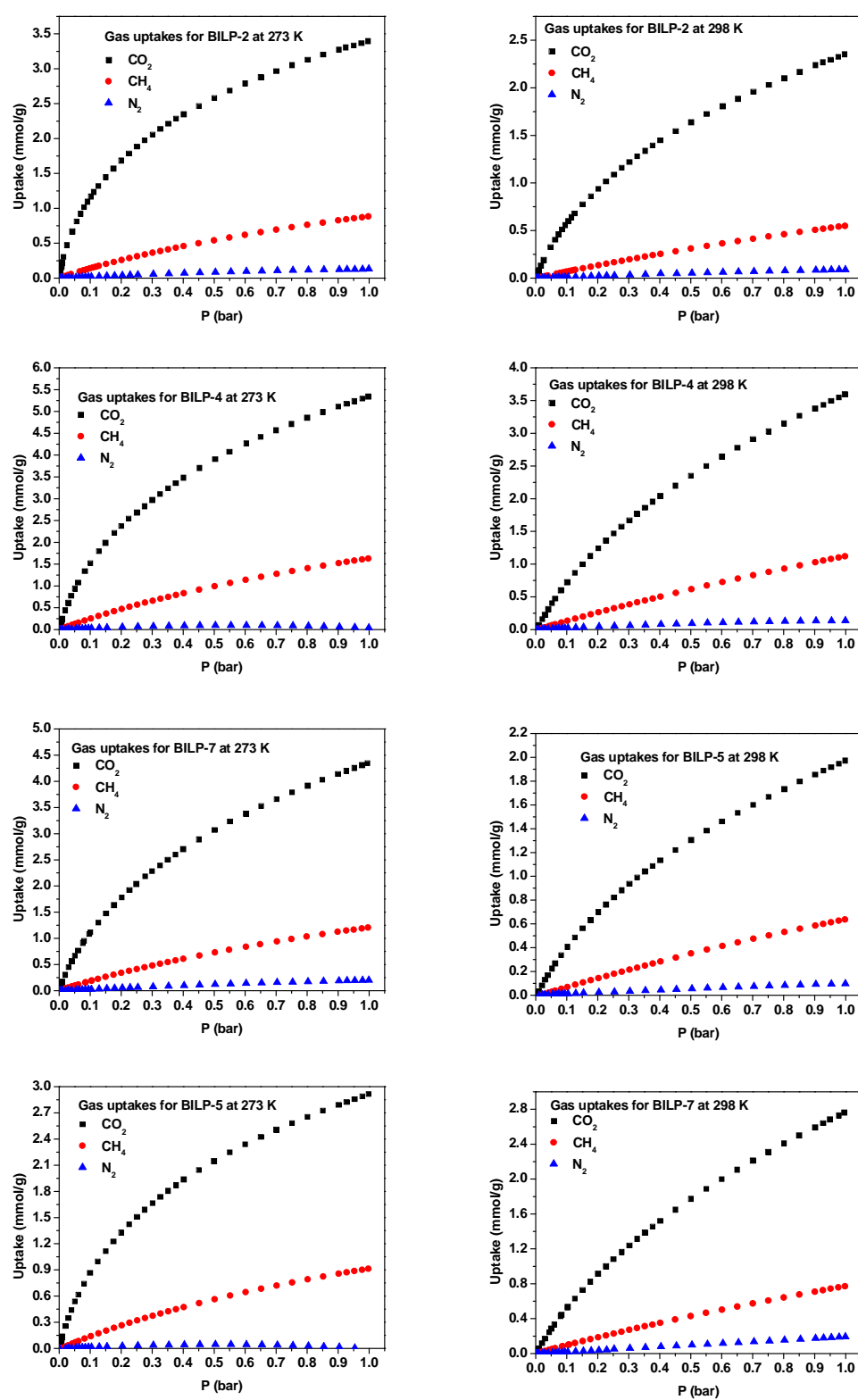


Figure S17: Adsorption selectivity of CO₂ over N₂ and CH₄ for BILPs from initial slope calculations.

CO₂ (black), CH₄ (red) and N₂ (blue) isotherms collected at 273 K and 298 K.

